RESEARCH ARTICLE

Climate-induced shift of deep-sea benthic foraminifera at the onset of the mid-Brunhes dissolution interval in the northeast tropical Indian Ocean

Hiroyuki Takata[1], Minoru Ikehara[2], Koji Seto[3], Hirofumi Asahi[4], Hyoun Soo Lim[5], Sangmin Hyun[6] and Boo-Keun Khim[7*]

Abstract

The mid-Brunhes dissolution interval (MBDI; Marine Isotope Stage (MIS) 13 to 7; ~ 533–191 ka) is characterized by various paleoclimatic/paleoceanographic events in the world. We investigated fossil deep-sea benthic foraminifera and sediment geochemistry at the onset of the MBDI (~ 670–440 ka) using Ocean Drilling Program (ODP) Site 758 and core GPC03 in the northeast tropical Indian Ocean (TIO), primarily focusing on the relationship between the paleoceanographic conditions of the surface and deep oceans. Based on multi-dimensional scaling, MDS axis 1 is related to the specific depth habitats of benthic foraminiferal fauna, possibly at the trophic level. In MDS axis 1, the difference between the two core sites was smaller from ~ 610 to 560 ka, whereas it was larger from ~ 560 to 480 ka. In contrast, MDS axis 2 may be related to the low food supply at episodic food pulses/relatively stable and low food fluxes. MDS axis 2 showed generally similar stratigraphic variations between the two cores during ~ 610–560 ka, but was different during ~ 560–480 ka. The proportion of lithogenic matter to biogenic carbonate was relatively low from ~ 610 to 530 ka under the highstand when sediment transport to the study area was reduced. Thus, both the depth gradient in the distribution of benthic foraminiferal fauna and the lithogenic supply between the two cores changed coincidently across the MIS 15/14 (~ 570–540 ka) transition. Such paleoceanographic conditions across MIS 15/14 transition were attributed to the long-term weakening of the wind-driven mixing of surface waters, which might have been caused by the weakening of the Indian summer monsoon in the northeast TIO, possibly with the northward displacement of the InterTropical Convergence Zone in the Northern Hemisphere. In particular, the depth gradient in the distributions of benthic foraminiferal faunas represents the paleoceanographic linkage between the surface and deep oceans through particulate organic matter ballasting by calcareous plankton skeletons in addition to lithogenic matter, which changed transiently and significantly across MIS 15/14 transition close to the onset of the MBDI.

Keywords Deep-sea biota, Sediment geochemistry, Ballasting effect, Wind-driven mixing, Indian summer monsoon, InterTropical Convergence Zone

*Correspondence:
Boo-Keun Khim
bkkhim@pusan.ac.kr
Full list of author information is available at the end of the article

Springer Open

Takata *et al. Progress in Earth and Planetary Science* (2024) 11:30

Page 2 of 18

1 Introduction

The duration from Marine Isotope Stage (MIS) 15 to 11 (621–374 ka) is the transitional period between the mid-Pleistocene Transition (MPT, ~1250–700 ka; Pisias and Moore 1981) and the mid-Brunhes dissolution interval (MBDI) (MIS 13 to 7; ~533–191 ka). The MBDI represents global carbonate dissolution, lasting several hundred thousand years, centered around MIS 11 (~424–374 ka; Barth et al. 2018) which is characterized by paleoceanographic/paleoclimatic events recognized in the surface and deep oceans (e.g., Jansen et al. 1986; Farrell and Prell 1989). The mid-Brunhes event was defined as a climatic shift, evidenced by marine sediments and Antarctic ice cores, between MIS 12 and 11 at approximately 430 ka, showing an increase in the amplitude of glacial-interglacial cycles (EPICA community members 2004). Recently, the mid-Brunhes Transition (MBT) has been proposed as a two-stage (MBT-1 and MBT-2) global climate shift and these two stages were distinguished by global and regional paleoclimatic/paleoceanographic events (Ao et al. 2020). The first stage (MBT-1) at ~500 ka was generally characterized by the regional phenomena during MIS 13 (533–478 ka). In this period, asymmetrical temperature and precipitation between the hemispheres and northward displacement of InterTropical Convergence Zone (ITCZ) in the Northern Hemisphere were reported. By contrast, the second stage (MBT-2) at ~400 ka was characterized by more global extents of paleoclimatic/paleoceanographic events from MIS 11. Yu et al. (2017) suggested that MIS 14 (563–533 ka) was uniquely interglacial-like, showing more sluggish Atlantic Meridional Ocean Circulation in the North Atlantic, northward shift of the ITCZ, and southward displacement of westerlies in the southeastern Pacific. In addition, Barth et al. (2018) suggested several sequential steps of global climatic events during MIS 15–11. Thus, the transitional period from MIS 15 to 11 is important in delineating the onset of the MBDI, particularly, focusing on the spatiotemporal variation of paleoclimatic/paleoceanographic events.

Due to differences in insolation, the sea surface temperature (SST) is relatively high in modern tropical oceans. The thermal contrast between the tropical and polar regions is a primary driving force of meridional atmospheric circulation such as the Hadley Circulation (e.g., Farrell 1990). In addition, the east–west gradient of the SST in the tropical ocean often causes interannual variations in atmospheric circulation (i.e., Walker Circulation) such as the El Niño-Southern Oscillation (ENSO) in the equatorial Pacific Ocean (Messie and Chavez 2013). Similar to modern circulation in the high SST tropical oceans (e.g., Fedorov et al. 2015), both the long-term (millions of years scale order) meridional and zonal atmospheric circulations might have been present in the geological past. For example, since the middle Pleistocene, the different decreasing SST trend between the eastern and western equatorial Pacific Ocean has resulted in an ENSO-like asymmetric zonal pattern along the equator through the intensity changes of the trade winds (e.g., Lie and Herbert 2004). The eastern tropical Indian Ocean (TIO), located in the Indo-Pacific Warm Pool (IPWP), plays an important role as a heat source that controls the global climate (e.g., De Deckker 2016), revealing that the spatiotemporal variation of paleoclimatic/paleoceanographic events related to long-term atmospheric circulation change in the TIO during the transitional period (MIS 15–11) is a possible driver of global climatic change.

Because deep-sea biota are sensitive to environmental conditions, as well as plankton and neritic organism, they have been used to evaluate the biodiversity of deep-sea microfossils in response to climatic change (e.g., Yasuhara et al. 2017). Benthic foraminifera provide crucial information on past trophic conditions (e.g., Gooday 2003; Jorissen et al. 2007). Benthic foraminiferal data have also been utilized to evaluate the ballasting effect of particulate organic matter (POM) on food delivery to the seafloor by mineral grains such as plankton skeletons (e.g., Griffith et al. 2021). Takata et al. (2019) studied the benthic foraminiferal faunas in the central equatorial Pacific Ocean and reported that the shift in the ballasting of POM from calcareous to siliceous plankton across ~300 ka. Takata et al. (2022) investigated the benthic foraminiferal faunas in the northeast TIO and found that changes in the ballasting of POM by calcareous plankton skeletons occurred at around 370–210 ka. Such a paleoceanographic event may be related to a long-term change in the asymmetric zonation of wind-driven upwelling between the eastern and western TIO, similar to the modern Indian Ocean Dipole mode (Takata et al. 2024). Since the ballasting of POM by mineral grains is an important mechanism for linking the paleoceanographic change between the surface and deep oceans, the ballasting effects of POM can be evaluated by the variation in benthic foraminiferal fauna in the deep-sea environment, which implies that atmospheric circulation changes influence the surface ocean conditions.

In this study, we investigated benthic foraminiferal fauna and measured the major elemental compositions of bulk sediments in terms of the depth transect at Ocean Drilling Program (ODP) Site 758 and core GPC03 in the northeast TIO, adjacent to the IPWP, during MIS 16–12 corresponding to the transitional period between the MPT and MBDI. The main objective of this study was to trace the paleoceanographic event at the onset of the MBDI in the northeast TIO by evaluating the ballasting effect of POM by mineral grains.

2 Methods

Oceanography in the Bay of Bengal is characterized by the distinct seasonality of wind and precipitation by the Indian monsoon, and the consequent large amount of freshwater discharge, transporting lithogenic particles from the Ganga–Brahmaputra–Meghna (GBM) River system. Rixen et al. (2019) observed seasonal variations in particulate organic carbon (i.e., POM) flux. The summer flux was high at Station SBBT (Southern Bay of Bengal Trap), which is located at a latitude similar to that of our study area (Fig. 1). In addition, Zhang et al. (2022) summarized carbonate sedimentation with water depth in the Indian Ocean, whereas the Bay of Bengal is exceptional area on the relationship between carbonate sedimentation and water depth because of dilution by the abundant lithogenic matter supply from the GBM River system. The Indian summer monsoon is driven by the different heating between the warmer Asian continent and the cooler Indian Ocean with the seasonal movements of the ITCZ (e.g., Webster et al. 1998).

ODP Site 758 (5°21′N, 90°21′E; water depth 2925 m) was drilled at the Ninetyeast Ridge during Leg 121

Fig. 1 Locality maps of our study area with ODP Site 758 and core GPC03 ([**a**] and its close-up [**b**])

(Fig. 1). A piston core GPC03 (length 956 cm; 5°20.84′N, 88°50.01′E; water depth 3650 m) was collected adjacent to ODP Site 758 in July 2018 during the HI1808 cruise by R/V ISABU (Fig. 1). Thirty-seven samples were taken from 9.9 to 6.3 mbsf (meters below sea floor: 11.7–7.6 mcd [meters composite depth]) at ODP Site 758 Hole A. From core GPC03, thirteen samples were obtained between 766 and 646 cm. The sediment lithology of both sampling intervals consisted of mainly calcareous nannofossil ooze (Shipboard Scientific Party 1989; Takata et al. 2022). The sediment samples were freeze-dried for laboratory analyses.

For the faunal analysis of benthic foraminifera, 2–6 g of freeze-dried sediment were processed following the protocol of Takata et al. (2022). More than 200 benthic foraminiferal specimens were picked, using a binocular microscope, in the > 105 μm fraction from split aliquots (1/2 to 1/32) of the washed residues (> 63 μm) that was followed by Nomura (1995). There are several opinions about the suitable size fraction and counting number for faunal analysis of benthic foraminifera (e.g., Boltovskoy and Wright 1976; Thomas 1985). Some scientists have adopted the > 150 μm fraction for benthic foraminiferal fauna, providing convenient identification, whereas other scientists have stated that the > 63 μm is more useful to catch the occurrences of the smaller taxa (e.g., phytodetritus species; Thomas 1985). In addition, many scientists have thought that the 100–300 counts are suitable for the reliable faunal analysis, as Boltovskoy and Wright (1976) mentioned. Nonetheless, there are variable ideas on the suitable size fraction and counting number of benthic foraminifera. In this study, we adopted the > 105 μm fraction and the 200 counts, following the same scheme of our previous studies (Takata et al. 2022, 2024). It allows the combination of the previous results with this study, which highlights the difference in paleoceanography between our study period and the younger span. The specimens were identified, and counted, following taxonomic assignments on Boltovskoy (1978), Corliss (1979), van Morkhoven et al. (1986), Jones (1994), and Nomura (1995), with the generic classification of Loeblich and Tappan (1987). We combined the new 13 data of core GPC03 with the published 34 data between 841 and 595 cm by Takata et al. (2022).

We examined the structure of community for each sample: rarefaction (diversity E [Sn]; n = 50), Shannon–Wiener function (H′) (Shannon and Weaver 1949), and the evenness of Buzas and Gibson (1969). We conducted non-metric multi-dimensional scaling (MDS) for a data matrix of relative abundance (25 taxa and 63 samples), following protocol and configuration of Takata et al. (2022). Calculation of the rarefaction and non-metric multi-dimensional scaling were performed, using the
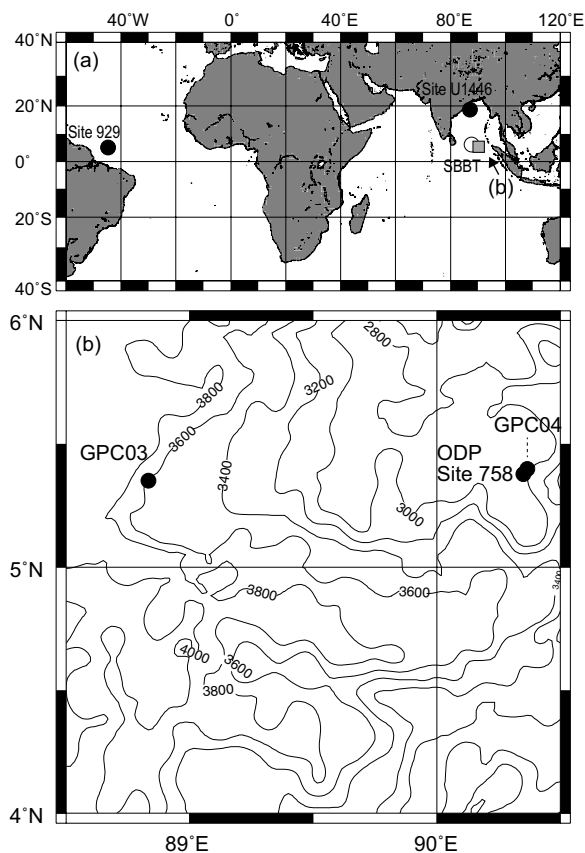
Takata *et al. Progress in Earth and Planetary Science*   (2024) 11:30

Page 4 of 18

statistical programming environment R (R Development Core Team 2020) with the function from the Vegan Community ecology package (Oksanen et al. 2019), whereas Shannon–Wiener function (H′) and the evenness were calculated via Microsoft Excel software.

For 34 samples from ODP Site 758, the concentrations of 11 major elements (Na_2O, MgO, SiO_2, Al_2O_3, P_2O_5, S, K_2O, CaO, TiO_2, MnO, and Fe_2O_3) were measured from a briquette, using an energy-dispersive X-ray fluorescence (XRF) elemental analyzer (MESA-500W, Horiba Co., Ltd.), following protocols and analytical conditions of Takata et al. (2024). The weight percentages of the 11 major elements were quantified using the standard regression method, based on the 12 standards provided by Dr. H. Fukusawa (former professor at Tokyo Metropolitan University, Japan). As chlorides were not removed from the sediment samples by rinsing with distilled water, the Na_2O data may be slightly overestimated.

In order to objectively evaluate the variations in the 10 elements (except for P_2O_5), we conducted a R-mode principal component (PC) analysis using the "prcomp" function in the statistical programming environment R (R Development Core Team 2020) based on a data matrix of the 10 elements and 33 samples. A sample at 8.48 mcd of ODP Site 758, which is relatively high SiO_2 probably due to one of thin ash layers (Shipboard Scientific Party 1989), was excluded from the principal component analysis. The correlation coefficient was used to calculate the diagonal matrix.

The $\delta^{18}O$ and $\delta^{13}C$ values of benthic foraminifera (*Cibicidoides wuellerstorfi*; > 250 μm fraction) from 31 samples of ODP Site 758 were measured at the Marine Core Research Institute of Kochi University (Japan). Two to five specimens were analyzed using an Elementar isoprime precisION with the Multicarb preparation system, reacting the samples with 100% phosphoric acid at 90 °C for 10 min. The data were calibrated to the VPDB standard using IAEA-603 and JCp-1 (Geological Survey of Japan) standards. The analytical precision (± 1σ) was ± 0.16‰ for $\delta^{18}O$ and ± 0.13‰ for $\delta^{13}C$. Takata et al. (2022) reported isotopic data for *C. wuellerstorfi* in core GPC03. In this study, the isotope values of *C. wuellerstorfi* (> 250 μm fraction) were additionally measured for new 13 samples of core GPC03 at the Oregon State University (USA) following the protocol of Takata et al. (2022). The analytical precision (± 1σ) was ± 0.02‰ for $\delta^{18}O$ and ± 0.04‰ for $\delta^{13}C$.

The orbitally-tuned age models at ODP Site 758 and core GPC03 were established by oxygen isotope stratigraphy. Isotope data at our study sites were standardized (zero mean and unit variance) prior to their correlation to global stack LR04 (Lisiecki and Raymo 2005). Stratigraphic correlation was performed under hidden Markov model (HMM) probabilistic algorithm (Lin et al. 2014; Ahn et al. 2017). This personal computer-based technique provides age model uncertainties of oxygen isotope alignment from every probabilistic match, as shown in Fig. 2. The assessments of age model uncertainty at ODP Site 758 and core GPC03 help heavily on our discussion on up-downs of mass accumulation rate (MAR).

For ODP Site 758, we calculated the MAR of Al_2O_3 and CaO at ODP Site 758 as follows: Al_2O_3-MAR or CaO-MAR (g cm^{-2} kyr^{-1}) = %(Al_2O_3 or CaO)/100 × LSR × DBD, where LSR is the linear sedimentation rate (cm kyr^{-1}) and DBD is the dry bulk density (g cm^{-3}) of the sediment. The DBD was obtained from the Shipboard Scientific Party (1989) by interpolation to our
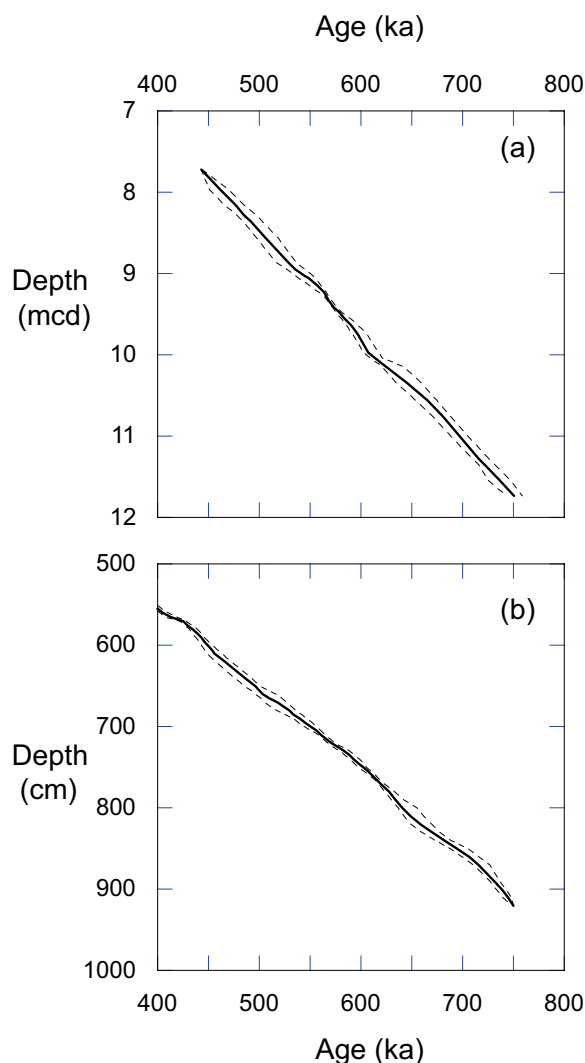

Fig. 2 Age-depth plots at ODP Site 758 (**a**) and core GPC03 (**b**). Dashed lines represent both the upper and lower 95% confidence ranges

samples based on core depths (mbsf) of the same hole (Hole A). We also calculated the benthic foraminiferal accumulation rate (BFAR; Herguera and Berger 1991), following the equation of Herguera and Berger (1991): BFAR (# cm^{-2} kyr^{-1}) = (the number of benthic foraminifera per unit gram of bulk sediment [# g^{-1}]) × LSR × DBD.

3 Results

The δ^{18}O and δ^{13}C values of *Cibicidoides wuellerstorfi* at ODP Site 758 ranged between 2.7–3.9‰ and − 0.5–0.4‰, respectively (Table S1; Fig. S1). On the other hand, those of core GPC03 ranged between 2.6–4.6‰ and − 0.9–0.5‰, respectively. Based on the matching of the oxygen isotope profiles to the LR04 stack, the age-depth curves with 95% confidence intervals for ODP Site 758 and core GPC03 are shown in Fig. 2.

Fossil benthic foraminifera were found in all samples in this study. The abundances of benthic foraminifera per unit weight at ODP Site 758 and core GPC03 ranged from 89 to 301 and 63 to 407, respectively (Fig. 3). *Oridorsalis umbonatus*, *Gyroidinoides* sp. A, *Pullenia* spp., *Epistominella exigua*, *Nuttallides umbonifer*, and *Eilohedra levicula* were common constituents in both cores, auxiliary to *Uvigerina dirupta*, *Siphouvigerina ampullacea*, *Globocassidulina subglobosa*, *Cibicidoides mundulus*, and *Astrononion echolsi* (Figs. 3, 4, 5). Obvious features on destruction or abrasion of the benthic foraminiferal tests were not observed both at ODP Site 758 and core GPC03 (Figs. 4, 5), similar to the observation of Takata et al. (2022, 2024). These features imply that the faunas are unlikely to be affected by downward transport from other areas to the core sites. In addition, severe carbonate dissolution was not detected on the benthic foraminiferal tests (Figs. 4, 5).

The faunal associations of benthic foraminifera were generally similar between the two cores, whereas some taxa differed in their stratigraphic distributions between the cores. For example, the relative abundances of uvigerinids, including *Siphouvigerina ampullacea*, were more common and *O. umbonatus* was less common at ODP Site 758 than in core GPC03 (Fig. 3). Both rarefaction (E[S$_{50}$]) and Shannon–Wiener (H′) of benthic foraminiferal fauna show frequent fluctuations in ODP Site 758 and GPC03 (Fig. 6). In addition, the species diversity indices at ODP Site 758 were partially higher than those of core GPC03, especially at ∼ 630 ka and ∼ 490 ka. The evenness of Buzas and Gibson (1969) was not markedly different between the two cores but varied significantly with depth (Fig. 6).

Two MDS axes were recognized in the benthic foraminiferal faunas. The scores of MDS axis 1 at ODP Site 758 were generally positive, whereas those of core GPC03 were negative (Fig. 6), suggesting a depth gradient

in the distribution of benthic foraminiferal fauna between the two cores. The scores of MDS axis 2 showed similar variation patterns between the two cores during MIS 15, whereas they showed different variation pattern during MIS 14–13 (Fig. 6). MDS axis 1 was positively correlated with *Gyroidinoides* sp. A and negatively correlated with *O. umbonatus* and *Pullenia jarvisi*, whereas MDS axis 2 is positively correlated with *C. mundulus* and negatively correlated with *E. exigua* and *N. umbonifer* (Table S2).

Among the elemental compositions of the bulk sediments at ODP Site 758, SiO$_2$ and CaO were the dominant components and Al$_2$O$_3$ and Fe$_2$O$_3$ were associated (Fig. 7; Table S1). The stratigraphic variation pattern of %CaO was generally opposite to those of %SiO$_2$, %Al$_2$O$_3$, %TiO$_2$, and %Fe$_2$O$_3$ (Fig. 7). According to the principal component analysis, the contributions of PC axes 1, 2, and 3 were 55.9%, 16.1%, and 11.4%, respectively. Due to the similarly low contributions of PC axes 2 and 3, we focused only on PC axis 1 in this study. PC axis 1 was characterized by positive loadings of SiO$_2$, Al$_2$O$_3$, TiO$_2$, and Fe$_2$O$_3$ and negative loading of CaO (Table 1). The former combination consists of a common elemental component in lithogenic matter such as illite and smectite, whereas the latter represents carbonates, particularly biogenic skeletons. These results suggest that the variation of PC axis 1 depends on the proportion of lithogenic detrital particles and biogenic carbonates. The PC axis 1 scores were normally more positive during MIS 17–16 and MIS 13–12, whereas they were more negative during MIS 15–14 (Fig. 7). With respect to PC axis 1 loadings, positive scores represented a greater contribution of lithogenic matter, whereas negative scores symbolized more biogenic carbonate contributions.

4 Discussion

4.1 Benthic foraminiferal faunas in the northeast tropical Indian Ocean

4.1.1 Faunal composition

We considered the ecological issues on the two MDS axes, based on ecological information on modern benthic foraminifera from Supplementary file 5 of Takata et al. (2022) and the literatures listed in Takata et al. (2024). Based on the correlation between the score on MDS axis 1 and the relative abundance of each taxon (Table S2), MDS axis 1 is negatively correlated to *Oridorsalis umbonatus* and *Pullenia jarvisi* and positively correlated to *Gyroidinoides* sp. A. These cosmopolitan taxa live at various water depths and trophic conditions (e.g., van Morkhoven et al. 1986). Peterson (1984) reported the spatial distribution of modern benthic foraminifera in the eastern equatorial Indian Ocean. According to his faunal list, both *O. umbonatus* and *Gyroidinoides orbicularis* (likely equivalent to our *Gyroidinoides* sp. A) are widely
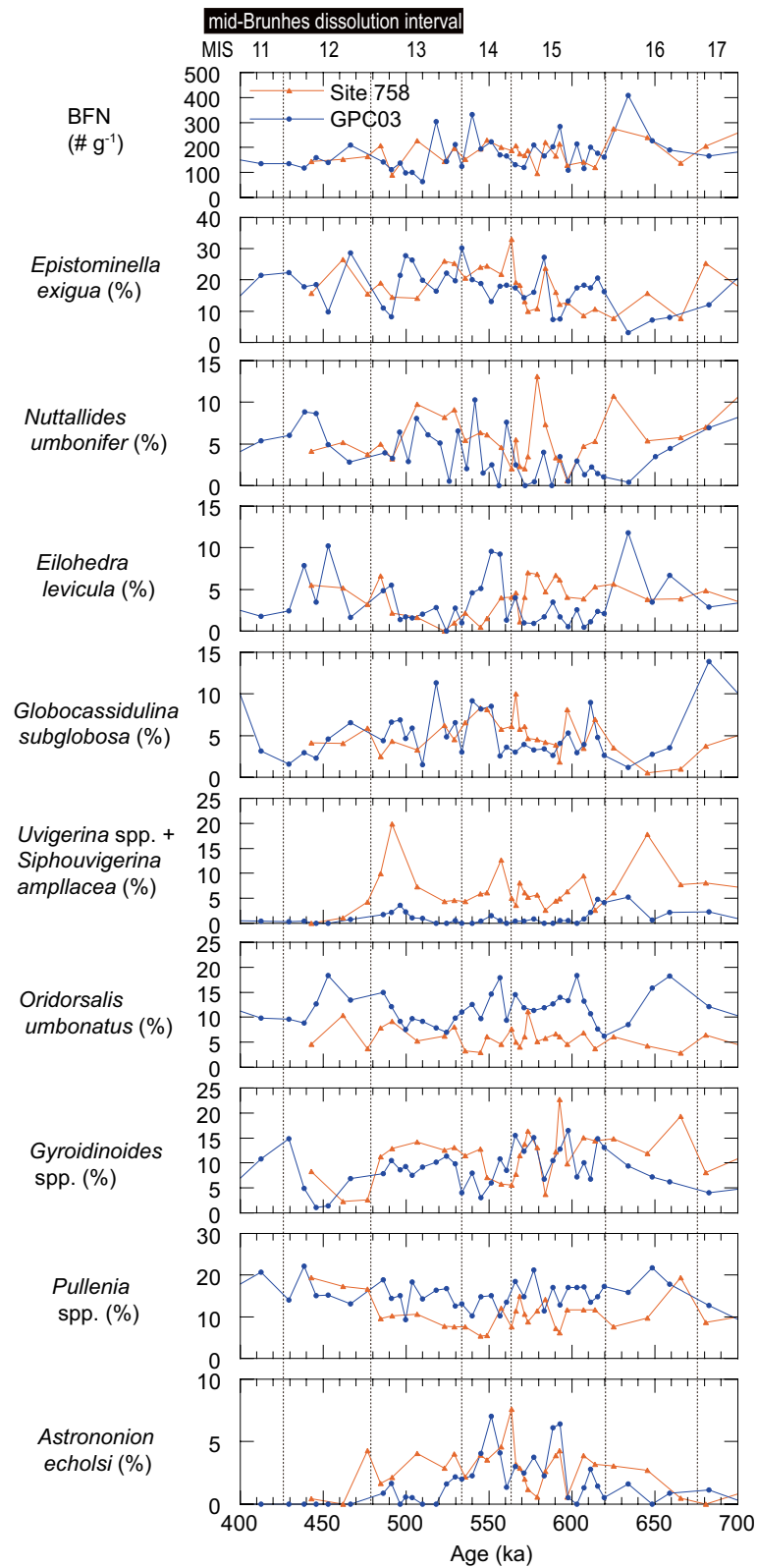
Fig. 3 Occurrences of benthic foraminifera. The abundance of benthic foraminifera per unit weight (BFN) and relative abundances of selected species of benthic foraminifera at ODP Site 758 (orange line) and core GPC03 (blue line) were shown
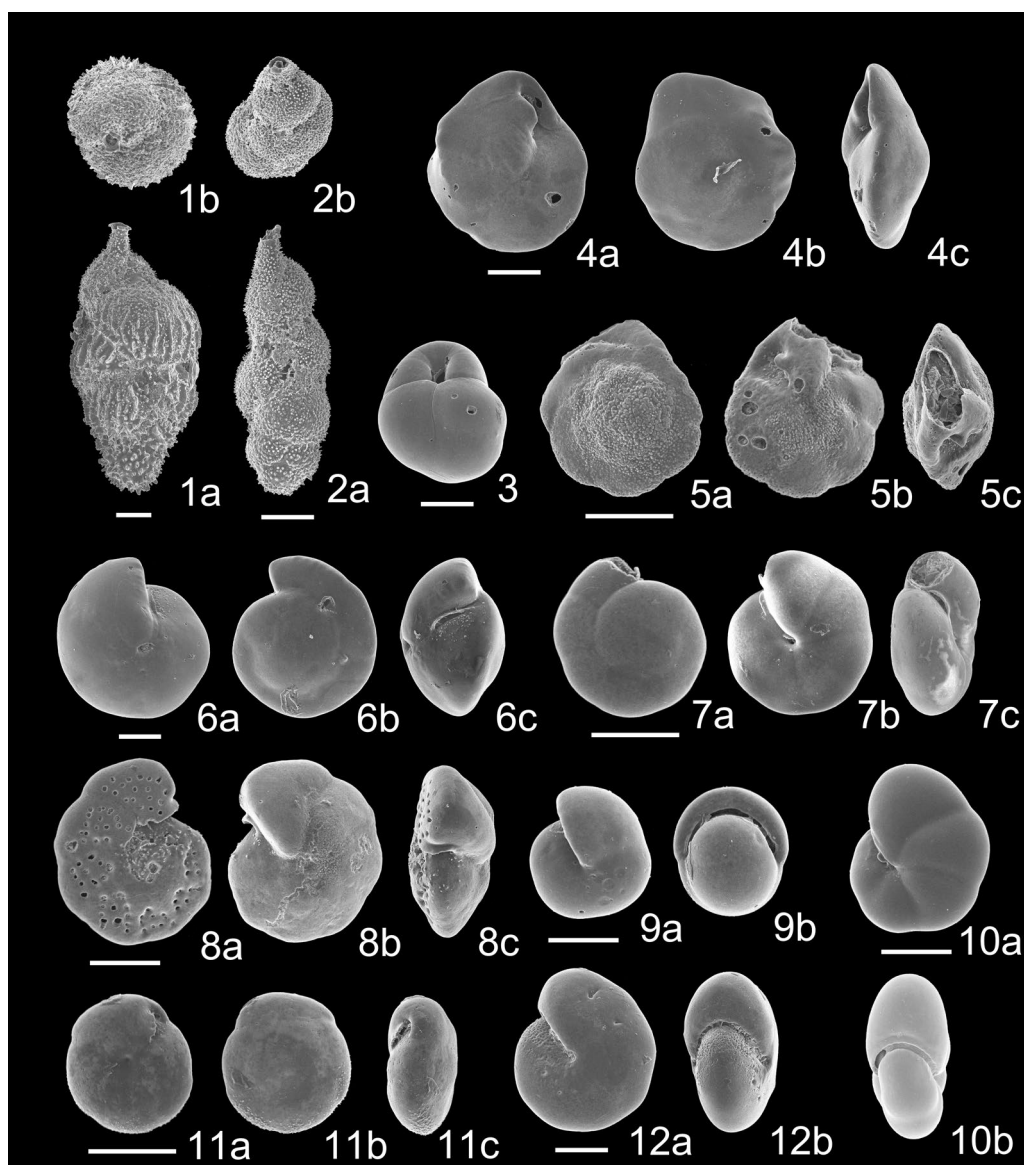
Fig. 4 Scanning electron micrographs of selected benthic foraminifera from ODP Site 758. Scale bars are 100 μm. 1a, b. *Uvigerina dirupta* from sample 758A-2H2-22-24 cm; 2a,b. *Siphouvigerina ampullacea* from sample 758A-2H1-92-95 cm; 3. *Globocassidulina subglobosa* from sample 758A-2H2-35-37 cm; 4a-c. *Epistominella exigua* from sample 758A-2H1-136-138 cm; 5a-c. *Nuttallides umbonifer* from sample 758A-2H1-113-116 cm; 6a-c. *Oridorsalis umbonatus* from sample 758A-2H2-48-50 cm; 7a-c. *Gyroidinoides* sp. A from sample 758A-2H1-113-116 cm; 8a-c. *Cibicidoides mundulus* from sample 758A-2H2-44-47 cm; 9a, b. *Pullenia bulloides* from sample 758A-2H2-40-42 cm; 10a, b. *Pullenia jarvisi* from sample 758A-2H2-22-24 cm; 11a-c. *Eilohedra levicula* from sample 758A-2H2-44-47 cm; 12a, b. *Astrononion echolsi* from sample 758A-2H2-29-32 cm

common at water depth of ~ 2000–4600 m, which cover the sampling water depths of our study sites (2925 m at ODP Site 758 and 3650 m at core GPC03). In the present study, the relative abundance of *O. umbonatus* was common during MIS 17–11 (Fig. 3). Takata et al. (2022) reported that its occurrence generally decreases after MIS 11. Thus, the past habitats of these species might have been different during MIS 16–12 compared to their modern distributions. It may be difficult to specify the

exact reason for their different occurrences during MIS 16–12 in the two cores, just based on modern ecological knowledge. In contrast, *Siphouvigerina ampullacea* was slightly positively correlated with MDS axis 1 (0.46) (Table S2). Other *Uvigerina* spp. were also more common at ODP Site 758 than at core GPC03 (Fig. 3). Uvigerinids are usually regarded as eutrophic taxa (e.g., Jorissen et al. 1997). Hence, although the interpretation of the ecological issue of MDS axis 1 is still difficult, the negative score
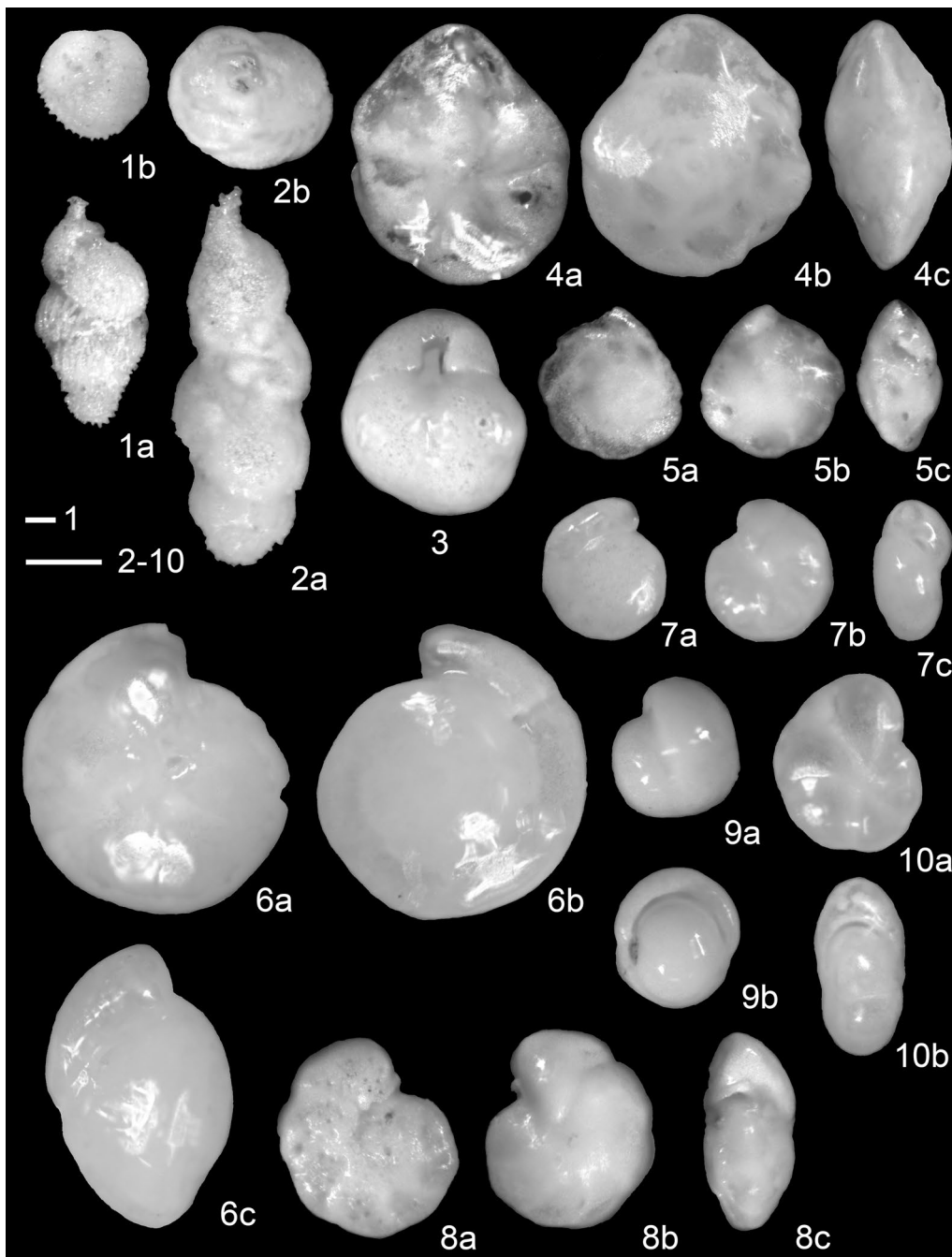
Fig. 5 Light micrographs of selected benthic foraminifera from ODP Site 758. Scale bars are 100 μm. 1a, b. *Uvigerina dirupta* from sample 758A-2H2-22-24 cm; 2a,b. *Siphouvigerina ampullacea* from sample 758A-2H1-92-95 cm; 3. *Globocassidulina subglobosa* from sample 758A-2H2-35-37 cm; 4a-c. *Epistominella exigua* from sample 758A-2H1-136-138 cm; 5a-c. *Nuttallides umbonifer* from sample 758A-2H1-113-116 cm; 6a-c. *Oridorsalis umbonatus* from sample 758A-2H2-48-50 cm; 7a-c. *Gyroidinoides* sp. A from sample 758A-2H1-113-116 cm; 8a-c. *Cibicidoides mundulus* from sample 758A-2H2-44-47 cm; 9a, b. *Pullenia bulloides* from sample 758A-2H2-40-42 cm; 10a, b. *Pullenia jarvisi* from sample 758A-2H2-22-24 cm

on MDS axis 1 was related to deeper water habitats of benthic foraminiferal fauna, especially at deep site (core GPC03) during MIS 16–12, whereas a positive score was related to shallower water habitats possibly with a relatively higher food supply.

MDS axis 2 was negatively correlated with *Epistominella exigua* and *Nuttallides umbonifer* and positively correlated with *Cibicidoides mundulus* (Table S2). *Epistominella exigua* is known as a common species with an episodic food supply (Gooday 1994;
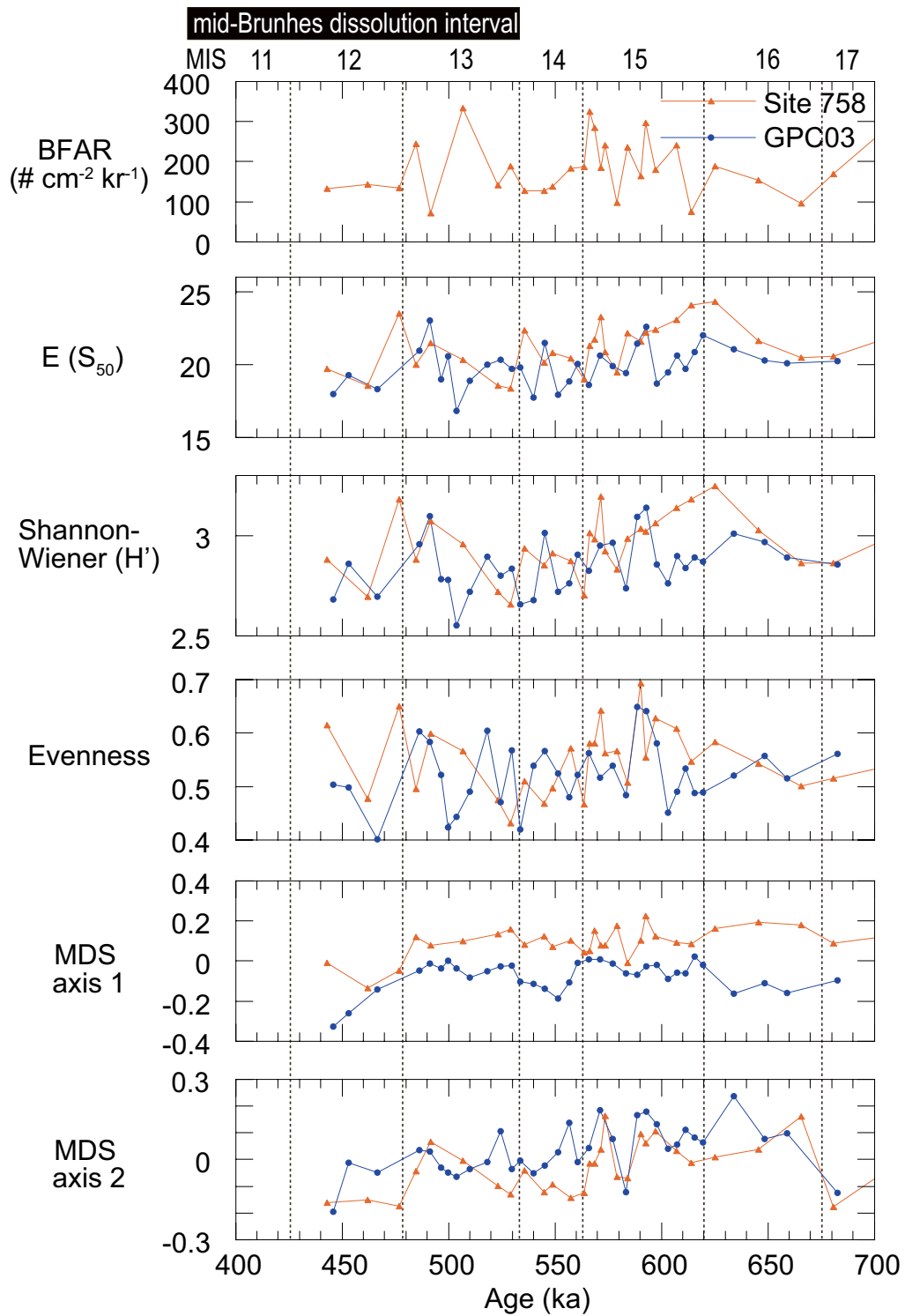
Fig. 6 Stratigraphic variations of benthic foraminiferal accumulation rate (BFAR) and the structure of the community, and multi-dimensional scaling. Rarefaction (E[S_{50}]), Shannon–Wiener index (H') evenness of Buzas and Gibson (1969), and scores of MDS axis 1 and 2 at ODP Site 758 (orange line) and core GPC03 (blue line) were shown
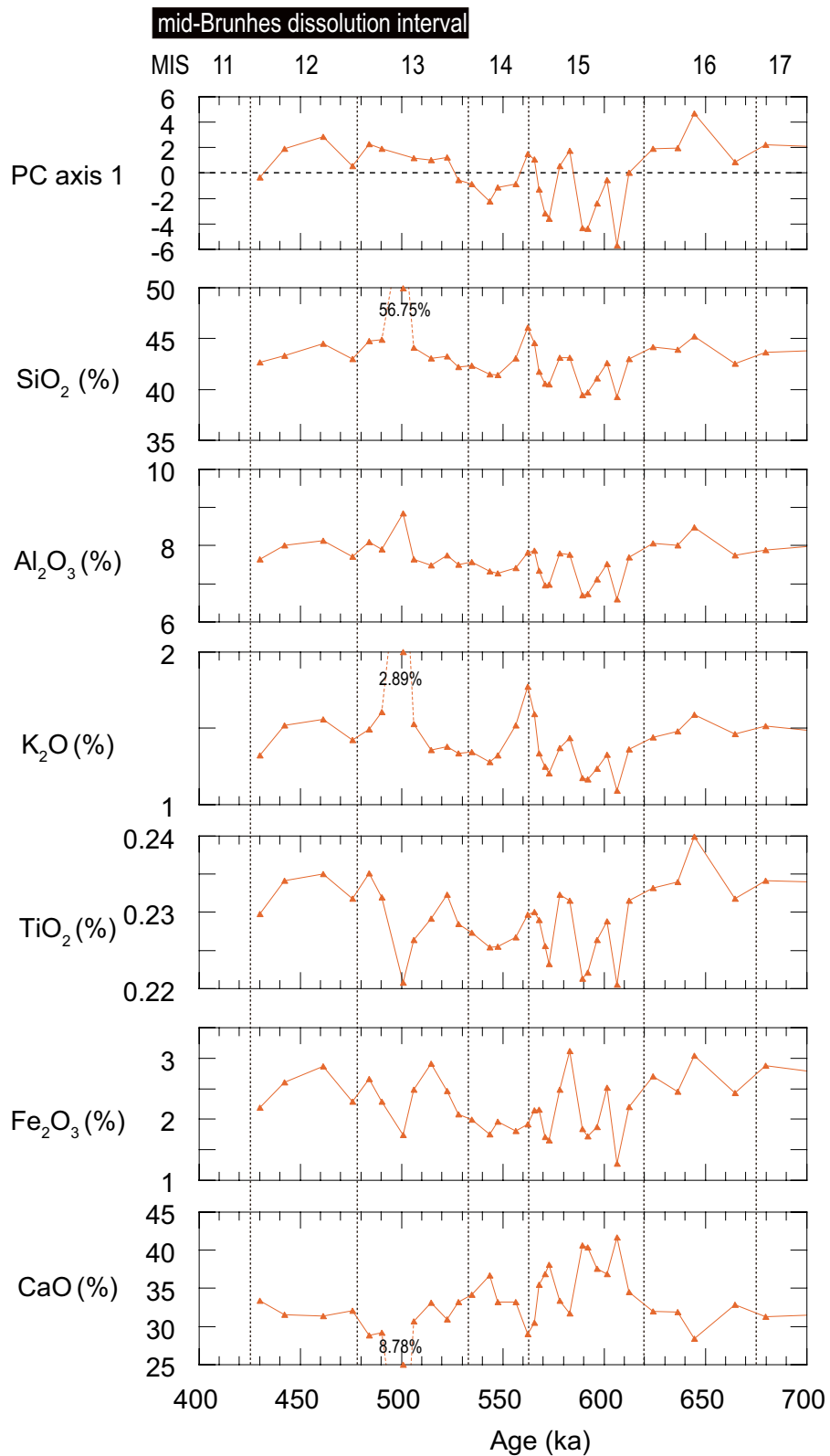
Fig. 7 Stratigraphic variations of PC axis 1 and selected 7 major elements at ODP Site 758

Table 1 Loadings of ten elements for PC axis 1 at ODP site 758

Element	Na_2O	MgO	Al_2O_3	SiO_2	S	K_2O	CaO	TiO_2	MnO	Fe_2O_3
PC axis 1	− 0.22	0.62	0.98	0.93	0.30	0.85	− 0.94	0.94	0.15	0.87

Smart et al. 1994; Thomas et al. 1995; Thomas and Gooday 1996; Sun et al. 2006; Thomas 2007; Takata et al. 2016). Many studies have reported that *Nuttallides umbonifer* occurred at abyssal depths between the lysocline and the calcium carbonate compensation depth (CCD) (Bremer and Lohmann 1982; Mackensen et al. 1990, 1993, 1995; Schmiedl et al. 1997). This species also tolerates an extremely low food supply (Schmiedl et al. 1997) in the greater depths where the organic matter reaches only a very small portion from surface ocean to the seafloor in general (Martin et al. 1987; Rigwell 2003; Henson et al. 2012; Griffith et al. 2021). *Nuttallides rugosa* (probably equivalent to *N. umbonifer*) was reported at ~1916 m water depth of the western Arabian Sea (Kurbjeweit et al. 2000). However, this species is commonly associated with low and seasonal food supplies (Gooday 1994, 2003; Sun et al. 2006), possibly due to its tendency to reproduce in such season. De and Gupta (2010) found *N. umbonifera* and *E. exigua* at the abyssal depths of the eastern and central Indian Ocean, which is characterized by carbonate-corrosive cold bottom waters and a low and pulsed food supply. However, *C. mundulus* is common under oligotrophic conditions (e.g., van Morkhoven et al. 1986), probably with a non-episodic (i.e., relatively stable) food supply, compared to *E. exigua*. Thus, a negative score on MDS axis 2 is likely related to an extremely low food supply with episodic food pulses, whereas a positive score may indicate a low but relatively stable food supply.

In summary, during our study period (MIS 16–12), MDS axis 1 was related to the specific depth habitats of benthic foraminiferal faunas possibly with trophic conditions in the tropical Indian Ocean, whereas MDS axis 2 may be related to food supply conditions. Thus, benthic foraminiferal fauna during MIS 16–12 seemed to be mainly influenced by water depth and episodic states of the food supply from the surface waters.

4.1.2 Depth gradient in the distributions of benthic foraminiferal faunas

Rarefaction ($E[S_{50}]$) and the Shannon–Wiener index (H′) at ODP Site 758 decreased slightly from late MIS 14 to early MIS 13, whereas those of core GPC03 did not vary distinctly (Fig. 6). The long-term changes in the species diversity of benthic foraminifera differed between the two sites. This suggests that the long-term changes in species diversity of benthic foraminifera occurred mainly at the shallow site (ODP Site 758; 2925 m water depth) rather than at the deep site (GPC03; 3650 m water depth). The difference in MDS axis 1 between the two cores was generally large during glacial periods (MIS 16 and 14; Fig. 8). In particular, MDS axis 1 during MIS 15 was similar, whereas that during MIS 14–13 was different (Fig. 6). Thus, the large difference in MDS axis 1 between the two cores seems to indicate an increased depth gradient in the distribution of benthic foraminiferal fauna. In contrast, MDS axis 2 showed a generally similar pattern of variation (small variation in the difference in MDS axis 2 in Fig. 8) between the two cores before MIS 15 (Fig. 6), whereas it was different (large variation in the difference in MDS axis 2 in Fig. 8) during MIS 14–13 (Fig. 6). Thus, based on both the structure of the community and the faunal composition represented by MDS axis 1, the depth gradient in the distribution of benthic foraminiferal faunas between ODP Site 758 and core GPC03 increased during MIS 14–13.

The lateral distance between ODP Site 758 and core GPC03, located at ~5°N is quite short (~168 km). Although we cannot dismiss the possibility of lateral distance on the oceanographic difference, it is reasonable to assume that the depth gradient in the distribution of benthic foraminiferal faunas seems to result from different water depths (~730 m difference) between the two sites. Such a depth gradient in the distribution of benthic foraminiferal faunas is difficult to comprehensively interpret based on modern ecological knowledge. However, this may be partly explained by the changes

(See figure on next page.)

Fig. 8 Stratigraphic variations of the several indices in this study. Mass accumulation rate (MAR) of CaO and Al_2O_3 and benthic foraminiferal accumulation rate (BFAR), sea-level change (Spratt and Lisiecki 2016), the differences of the scores of MDS axis 1 and 2 between ODP Site 758 and core GPC03, the relative abundance of *Globigerina bulloides* at ODP Site 758 (Chen and Farrell 1991), and relative abundance of *G. bulloides* (Bhadra and Saraswat 2022) and stable oxygen isotope variations of seawater that was estimated by oxygen isotope values of planktonic foraminifera and TEX 86-sea surface temperature at IODP Site U1446 (Clemens et al. 2021) were shown
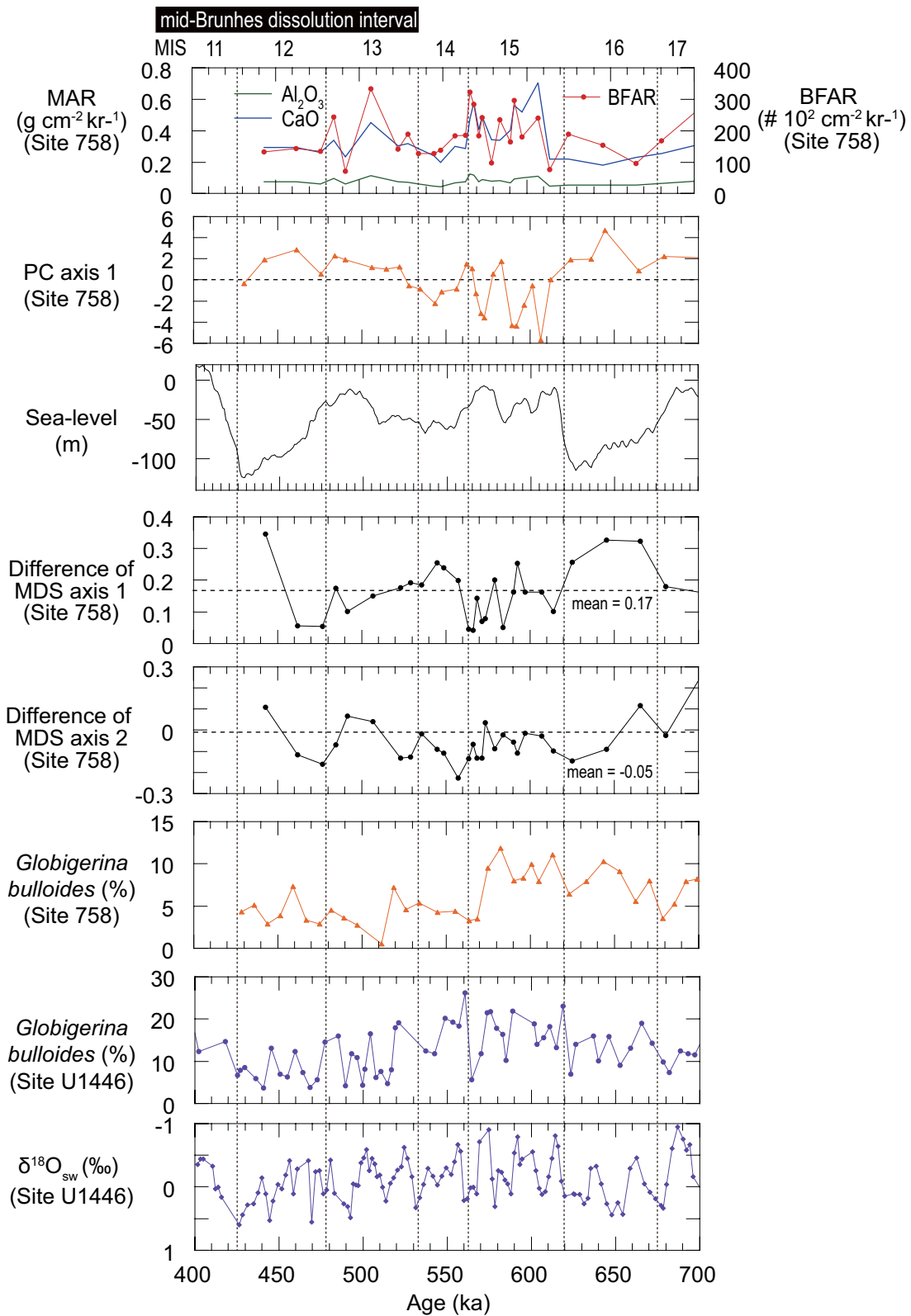
Fig. 8 (See legend on previous page.)

in water mass during the MIS 16–12. Peterson and Prell (1985) reported that the Composite Dissolution Index (CDI) was more negative (i.e., more carbonate-corrosive condition) in the equatorial Indian Ocean during MIS 13–11. The boundary between the Indian Deep Water (IDW) and Indian Bottom Water (IBW) is currently roughly consistent with the lysocline (~3900–3800 m water depth) at present (Peterson 1984) where the CDI is almost 0 (Peterson and Prell 1985). Thus, during MIS 13–12, the boundary between the IDW and the IBW might be located shallower than the core GPC03 site (3650 m water depth), compared to the present day. Thus, the depth gradient in the distribution of benthic foraminiferal faunas between ODP Site 758 and core GPC03 was enhanced during MIS 13–12.

Howe and Piotrowski (2003) reported stratigraphic changes in ε_{Nd} at ODP Site 929 (western equatorial Atlantic) over the last ~800 ka (Fig. S2). The ε_{Nd} value in the Atlantic Ocean represents the proportion of AABW to NADW. This fluctuation in ε_{Nd} clearly indicates the orbital-scale glacial-interglacial variations, similar to LR04 stack of benthic $\delta^{18}O$ values (Lisiecki and Raymo 2005). However, they did not show a marked long-term tendency during the MBDI. On the other hand, Barth et al. (2018) reported a larger gradient of benthic $\Delta\delta^{13}C$ values between the North Atlantic and South Atlantic during the "pre-MBT (mid-Brunhes Transition)" than "post-MBT" (Fig. S2). They regarded the larger gradient of benthic $\Delta\delta^{13}C$ values as the northward penetration of AABW and the lower gradient as the southward penetration of NADW. They recognized that the gradient of benthic $\Delta\delta^{13}C$ values between the North Atlantic and South Atlantic changed at the beginning of MIS 12 (~436 ka), and this transition appears to be a gradual change during MIS 14–12 than an abrupt one (Fig. S2). This onset timing is generally consistent with our observation of an enhanced depth gradient of the MDS axes across MIS 14. Although careful interpretation is necessary, based on the $\Delta\delta^{13}C$ values between the North Atlantic and South Atlantic which indicate the different proportion of deep-water formation between the AABW and NADW, the enhanced depth gradient in the distribution of benthic foraminifera across MIS 14 might be related to the global deep-water circulation.

In summary, the specific depth distribution of benthic foraminifera represented by MDS axis 1 between ODP Site 758 and core GPC03 seems to be related to the shallower position of the boundary between the IDW and IBW in the Indian Ocean during MIS 16–12, compared to the modern ocean. In addition, changes in the depth distribution of benthic foraminifera across MIS 14 may reflect changes in global deep-water circulation.

4.2 Ballasting effect of particulate organic matter by mineral grain in the northeast tropical Indian Ocean prior to the onset of the mid-Brunhes dissolution interval

Sediment trap studies have reported the ballasting effect of particulate organic matter (POM) by mineral grains in the water columns of modern ocean (Francois et al. 2002; Henson et al. 2012; Rixen et al. 2019). Ballasting of POM by biogenic carbonate grains (calcareous plankton skeleton) may increase the transfer efficiency of POM from the surface waters to the seafloor (Francois et al. 2002). Benthic foraminiferal data have been used to evaluate the ballasting effects of POM by mineral grains (Diester-Haass and Faul 2019; Griffith et al. 2021; Takata et al. 2019, 2022). Takata et al. (2022) reported a positive correlation between BFAR and carbonate-MAR in core GPC03 from ~600–370 ka (MIS 15–11) and after ~210 ka (mid-MIS 7), which suggests that calcareous plankton skeletons (probably mainly calcareous nanoplankton) affected the transfer efficiency of POM through the ballasting effect of POM in the northeast TIO. In our study interval (MIS 16–12), the correlation between the BFAR and CaO-MAR was positive (r = 0.66, P < 0.01) at ODP Site 758 (Fig. 8). Since the contribution of Ca-bearing silicates (e.g., illite) was very minor compared to biogenic carbonate (Takata et al. 2022), the positive correlation implies that calcareous plankton skeletons seem to promote the better transfer of sinking POM in the water column as ballast at ODP Site 758 during our study period (MIS 16–12).

In our study area, lithogenic matter was affected mainly by riverine input from the GBM Rivers (e.g., Zhang et al. 2022). In addition to calcareous plankton skeletons, lithogenic matter is thought to be an efficient ballasting material for POM sinking (Rixen et al. 2019). Takata et al. (2024) reported a positive correlation between %*N. umbonifer* and the contribution of lithogenic matter during the last ~450 ka, confirming the increasing ballasting effect of POM by lithogenic matter in the northeast TIO. At ODP Site 758, the correlation between BFAR and Al_2O_3-MAR was positive (r = 0.79, P < 0.01) during MIS 16–12 (Fig. 8). In addition to calcareous plankton skeletons, lithogenic matter such as illite-containing aluminum seemed to intensify the transfer efficiency of sinking POM in the water column as ballast at ODP Site 758 during MIS 16–12. Particularly, during MIS 15–14, PC axis 1 on the major elemental compositions related to lithogenic matter and biogenic carbonate was largely negative (Fig. 8), suggesting that the contribution of lithogenic matter was relatively low, compared to biogenic carbonate. Because this period is characterized by a relatively high sea level (Spratt and Lisiecki 2016; Fig. 8), the low contribution of lithogenic matter is due to the

distance from the mouths of the GBM Rivers to our study area.

The variation in PC axis 1 of the major elemental compositions showed short-term fluctuations during MIS 15 (Fig. 8). The timing of the negative scores of PC axis 1 in this period generally corresponded to relatively high sea levels at ∼ 610, ∼ 590, and ∼ 570 ka (Fig. 8). In addition, the scores of MDS axis 2 of benthic foraminifera were more positive and increased twice at ∼ 590 ka and ∼ 570 ka at both ODP Site 758 and core GPC03 (Fig. 6). It is reasonable to suppose that the small fluctuations of lithogenic matter supply may have resulted in more short-term positive scores on MDS axis 2 at both cores under the decreasing supply of lithogenic matter during MIS 15 due to the highstand. This low supply of lithogenic matter during MIS 15 may be attributed to frequent fluctuations in the episodic/more stable food supply from the surface waters to the seafloor.

The greater influence of lithogenic matter during MIS 14–13 may also explain the different variation patterns of MDS axis 2 between ODP Site 758 and core GPC03 (Fig. 8) through the efficiency of sinking POM in the water column. A shift to different variation patterns of the scores of MDS axis 2 between the two cores during MIS 14–13 implies that the food supply became more episodic (e.g., more seasonal variation) at the shallower site (ODP Site 758) than at the deeper site (core GPC03) (Fig. 8). The faunal transition from MIS 15 to MIS 14–13 may be attributed to the change from a more stable food supply to a more episodic food supply from the surface waters.

However, the relationship between PC axis 1 and %*N. umbonifer* at ODP Site 758 (Fig. 2) was not strong during our study period (MIS 16–12), compared with the younger interval (MIS 10–1) in core GPC04 which is located close to ODP Site 758 (Takata et al. 2024). The mode of the ballasting effect of POM by lithogenic matter in our study area seemed to differ between MIS 16–12 and the younger period (MIS 8–1). Thus, this seems to support the inference of Takata et al. (2024) that the influence of riverine lithogenic matter supply became significant for the vertical transportation of POM in our study area due to increased sea level lowering during glacial periods since MIS 8.

4.3 Paleoceanography in the northeast tropical Indian Ocean at the onset of the mid-Brunhes dissolution interval

Chen and Farrell (1991) reported planktonic foraminiferal fauna during the last ∼ 800 ka at ODP Site 758 (Fig. 8). According to their faunal data, the %*Globigerina bulloides* declined across MIS 14, despite the possible severe carbonate dissolution to planktonic foraminiferal fauna during MIS 15–14. This species is common in the upwelling regions of low-latitude oceans (e.g., Thiede 1975). Maeda et al. (2022) conducted a sediment trap study at Station CBBT-N (southwestern Bay of Bengal) and reported that *G. bulloides* was common during the monsoon periods (summer and winter) owing to the enhanced surface and subsurface primary production. This ecological evidence suggests that the decline of %*G. bulloides* at ODP Site 758 is related to decreased primary production due to the weakening of wind-driven mixing in the surface waters of the northeast TIO across MIS 15/14 transition. In contrast, Bhadra and Saraswat (2022) reported that %*G. bulloides* declined during MIS 14 at IODP Site U1446 (northern Bay of Bengal; 1441 m water depth), similar to ODP Site 758 (Fig. 8), despite high-amplitude short-term variations. They interpreted that the long-term declining trend of this species across MIS 14 was related to Indian summer monsoon variability. In addition, the estimated $\delta^{18}O$ values of seawater increased generally from MIS 15 to MIS 13, confirming the weakening of the Indian summer monsoon (Fig. 8; Clemens et al. 2021). Thus, the long-term declines of %*G. bulloides* at both IODP Site 1446 and ODP Site 758 in the Bay of Bengal suggests that the weakening of the Indian summer monsoon occurred in our study area across the MIS 15/14 transition, which might have caused the long-term weakening of wind-driven mixing in the surface ocean.

Across MIS 15/14 transition, changes in PC axis 1 (the proportion of lithogenic matter to biogenic carbonate) at ODP Site 758 and the depth differences in MDS axes 1 and 2 (benthic foraminiferal faunas) between ODP Site 758 and core GPC03 were observed (Fig. 8). Both changes between surface water oceanography (i.e., food production) and deep-sea biota (i.e., benthic foraminifera) were altered temporally and significantly across MIS 15/14 transition, possibly through the ballasting effect of POM by calcareous plankton skeletons and the lithogenic matter. Yu et al. (2017) reported that the "interglacial-like MIS 14" was a unique paleoceanographic setting, such as more sluggish Atlantic Meridional Ocean Circulation, and the northward shift in the ITCZ in the Northern Hemisphere. The weakening of the Indian summer monsoon across MIS 15/14 transition also seems be the paleoceanographic condition of "interglacial-like MIS 14" in the northeast TIO. The northward displacement of the ITCZ during MIS 13 (MBT-1) proposed by Ao et al. (2020) may also be related to the weakening of the Indian summer monsoon and subsequent faunal transition of deep-sea benthic foraminiferal in the northeast TIO across MIS 14. The weakening of the wind-driven mixing with the Indian summer monsoon is usually related to more southward seasonal movement of the ITCZ at the present day. On the other hand, the long-term weakening

of the wind-driven mixing in the northeast TIO with the Indian summer monsoon (as shown by *G. bulloides* at ODP Site 758 and IODP Site 1446) across MIS 15 to 13 transition seemed to be related to the global climatic change resulting from the asymmetric climatic variations between the Northern and Southern Hemispheres across MIS 14 (e.g., Hao et al. 2015). During this period, Ao et al. (2020) reported the northward displacement of the ITCZ in the Northern Hemisphere.

Yu et al. (2017) proposed the two hypotheses for the unique paleoceanographic setting of "interglacial-like MIS 14." The first hypothesis concerns on the influence of more nutrient-rich cold water from high latitudes via the Peru–Chile Current in the eastern equatorial Pacific (EEP). In addition, the magnitude of the EEP cold tongue weakened in the EEP through the atmospheric bridge of a northward ITCZ shift and the resulting heat/moisture transport across the eastern equatorial Atlantic (EEA). Another hypothesis is that the unique orbital variations in MIS 14 that were characterized by higher obliquity fluctuations and lower eccentricity/precession, resulting in an inter-hemispheric asymmetry. Both hypotheses can be applied to the northeast TIO to change the surface water oceanography and deep-sea benthic foraminiferal fauna.

Barth et al. (2018) summarized the multi-proxy data of multiple core sites in the world's ocean from the last ~800 ka by conducting principal component analyses. More positive excursion of $\delta^{13}C$ values of benthic foraminifera was distinct during MIS 13 (their PC axis 1 in Figs. 6 and 7). Such positive $\delta^{13}C$ excursion is significant in the Atlantic Ocean, but it is not obvious in the Pacific Ocean. More positive shift was not also distinct in our $\delta^{13}C$ values of *C. wuellerstorfi* in core GPC03 (Fig. S2). More positive excursion of $\delta^{13}C$ values of benthic foraminifera during MIS 13 was attributed to the unique setting of export productivity between the Antarctic zone and Subantarctic zone in the Southern Ocean (as shown in Fig. 9 of Barth et al. 2018). Barth et al. (2018) suggested that, during MIS 15–13, a build-up of Northern Hemisphere biomass as a result of accumulation of isotopically light carbon and enriched ^{13}C in the ocean due to Asian summer monsoon. In the Bay of Bengal, both %*G. bulloides* and estimated $\delta^{18}O$ values of seawater at IODP Site 1446 (Bhadra and Saraswat 2022; Clemens et al. 2021) imply stronger Indian summer monsoon during MIS 15 to 13 (Fig. 8), although their interpretation was partly inconsistent to the weakening of the Indian summer monsoon across MIS 15/14 transition in our study area. Further data evaluation of the Asian summer monsoon during MIS 15–13 is necessary to confirm Barth et al. (2018), who proposed sequential steps of paleoceanographic events related to the carbon cycle during

the MBDI. Finally, Takata et al. (2024) suggested that the benthic foraminiferal fauna in the northeast TIO could have been influenced by the Indian Ocean Dipole mode-like long-term transition during late MIS 9–8, following the scheme of Gupta et al. (2010). Similar paleoceanographic events may have affected the long-term changes in surface- and deep-sea conditions in the northeast TIO at the onset of the MBDI.

5 Conclusions

This study investigated fossil benthic foraminifera and sediment geochemistry at ODP Site 758 and core GPC03 in the northeast tropical Indian Ocean during MIS 16–12 and led to the following conclusions:

1. MDS axis 1 is related to the specific depth habitats of benthic foraminiferal fauna, possibly to the trophic condition in the TIO during MIS 16–12. The difference in MDS axis 1 between the two sites was smaller during MIS 15, but it was larger during MIS 14–13 because of the depth gradient in the distributions of benthic foraminiferal faunas. MDS axis 2 may be related to the low food supply with episodic food pulses/relatively stable low food flux. The variation pattern of this axis was generally similar during MIS 15 between the two cores but different during MIS 14–13. This indicates that the depth gradient between these two cores was intensified during MIS 14–13, which may be attributed to the shoaling boundary between the Indian Deep Water and Indian Bottom Water. Such a paleoceanographic event might be related to deep-water circulation changes in the Atlantic Ocean during the same period.

2. During the highstand across MIS 15/14 transition, changes in the proportion of lithogenic matter to biogenic carbonate represented by PC axis 1 at ODP Site 758 and the depth gradient in the distributions of benthic foraminiferal fauna between ODP Site 758 and core GPC03 were discernible. During such paleoceanographic events, the linkage between the surface and deep oceans was altered temporally and significantly, particularly across MIS 15/14 transition, mainly due to the ballasting effect of POM by calcareous plankton skeletons in addition to lithogenic matter.

3. The decrease of %*Globigerina bulloides* across MIS 15/14 transition represents the reduced primary production due to the weakening of wind-driven mixing in the surface ocean in our study area. Such paleoceanographic condition has been attributed to the long-term weakening of the wind-driven mixing in the northeast TIO with the Indian summer monsoon, possibly due to the northward displacement of

the InterTropical Convergence Zone across MIS15 to 13. The long-term weakening of the Indian summer monsoon across MIS 15/14 enhanced the depth gradient in the distribution of benthic foraminifera in the northeast TIO.

Abbreviations

AABW	Antarctic Bottom Water
BFAR	Benthic foraminiferal accumulation rate
CDI	Composite Dissolution Index
ENSO	El Niño-Southern Oscillation
GBM	Ganga–Brahmaputra–Meghna
IBW	Indian Bottom Water
IDW	Indian Deep Water
IODP	International Ocean Discovery Program
ITCZ	InterTropical Convergence Zone
MAR	Mass accumulation rate
MBDI	Mid-Brunhes dissolution interval
MBT	Mid-Brunhes Transition
MDS	Multi-Dimensional Scaling
MIS	Marine Isotope Stage
NADW	North Atlantic Deep Water
ODP	Ocean Drilling Program
POM	Particulate organic matter
SSBT	Southern Bay of Bengal Trap Station
SST	Sea surface temperature
TIO	Tropical Indian Ocean

Supplementary Information

The online version contains supplementary material available at https://doi.org/10.1186/s40645-024-00633-y.

Supplementary Material 1: Figure S1. Isotope stratigraphy in our study at ODP Site 758 and in core GPC03.

Supplementary Material 2: Figure S2. Stratigraphic variations of several proxy data in this study. Carbon isotope values of *Cibicidoides wuellerstorfi* in core GPC03, ε_{Nd} at ODP Site 929 (Howe and Piotrowski 2003), and $\Delta\delta^{13}C$ values between the North and South Atlantic Ocean (Barth et al. 2018) were shown.

Supplementary Material 3: Table S1. Weight percent of 11 major elements, score of PC axis 1, and stable oxygen and carbon isotope ratios of *Cibicidoides wuellerstorfi* at ODP Site 758

Supplementary Material 4: Table S2. Occurrences of fossil benthic foraminifera at ODP Site 758

Supplementary Material 5: Table S3. Correlation coefficient between MDS axes and each taxon; the results between MDS axis 1 or 2 and each taxon at ODP Site 758 and core GPC03

Availability of data and materials

The datasets supporting the conclusions of this article are included within its additional files.

Declarations

Competing interests

The authors declare that they have no competing interest.

Author details

[1]BK21 School of Earth and Environmental Systems, Pusan National University, 2 Busandaehak-ro 63 beon-gil, Busan 46241, Republic of Korea. [2]Marine Core Research Institute, Kochi University, B200 Monobe, Nankoku 783-8502, Japan. [3]Estuary Research Center, Shimane University, 1060 Nishikawatsu, Matsue 690-8504, Japan. [4]Fukui Prefectural Satoyama-Satoumi Research Institute, 122-12-1 Torihama, Wakasa 919-1331, Japan. [5]Department of Geological Sciences, Pusan National University, 2 Busandaehak-ro 63 beon-gil, Busan 46241, Republic of Korea. [6]Marine Environmental Research Department, Korea Institute of Ocean Science and Technology, 385 Haeyang-Ro, Busan 49111, Republic of Korea. [7]Department of Oceanography and Marine Research Institute, Pusan National University, 2 Busandaehak-ro 63 beon-gil, Busan 46241, Republic of Korea.

References

Ahn S, Khider D, Lisiecki LE, Lawrence CE (2017) A probabilistic Pliocene-Pleistocene stack of benthic $\delta^{18}O$ using a profile hidden Markov model. Dyn Stat Clim Syst 2017:1–16. https://doi.org/10.1093/climsys/dzx002

Ao H, Rohling EJ, Stringer C, Roberts AP, Dekkers MJ, Dupont-Nivet G, Yu J, Zhang P, Liu Z, Ma X, Zhou W, Jin Z, Xiao G, Wang H, Sun Q, Yang P, Peng Z, Shi Z, Qiang X, An Z (2020) Two-stage mid-Brunhes climatic transition and mid-Pleistocene human diversification. Earth Sci Rev 210:103354. https://doi.org/10.1016/j.earscirev.2020.103354

Barth AM, Clark PU, Nill NS, He F, Pisias NG (2018) Climate evolution across the Mid-Brunhes Transition. Clim past 14:2071–2087. https://doi.org/10.5194/cp-14-2071-2018

Bhadra SR, Saraswat R (2022) A strong influence of the mid-Pleistocene transition on the monsoon and associated productivity in the Indian Ocean. Quatern Sci Rev 295:107761. https://doi.org/10.1016/j.quascirev.2022.107761

Boltovskoy E (1978) Late Cenozoic benthonic foraminifera of the Ninetyeast Ridge (Indian) Ocean. Mar Geol 26:139–175

Boltovskoy E, Wright R (1976) Recent Foraminifera. Junk, The Hague

Bremer ML, Lohmann GP (1982) Evidence for primary control of the distribution of certain Atlantic Ocean benthonic foraminifera by degree of carbonate saturation. Deep-Sea Res 29:987–998

Buzas MA, Gibson TG (1969) Species diversity: benthonic foraminifera in western North Atlantic. Science 163:72–75

Chen M-T, Farrell J (1991) Planktonic foraminifer faunal variations in the north-eastern Indian Ocean: A high-resolution record of the past 800000 years from Site 758. In: Weissel J Peirce J, Taylor E, Alt J et al (eds) Proceedings of the ocean drilling program, scientific results, vol 121, College Station, pp 125–140

Clemens SC, Yamamoto M, Thirumalai K, Giosan L, Richey JN, Nilsson-Kerr K, Rosenthal Y, Anand P, McGrath SM (2021) Remote and local drivers of Pleistocene South Asian summer monsoon precipitation: a test for future predictions. Sci Adv 7:eabg3848. https://doi.org/10.1126/sciadv.abg3848

Corliss BH (1979) Taxonomy of recent deep-sea benthonic foraminifera from the Southeast Indian Ocean. Micropaleontology 25:1–19

De Deckker P (2016) The Indo-Pacific Warm Pool: critical to world oceanography and world climate. Geosci Lett 3:1–20

De S, Gupta AK (2010) Deep-sea faunal provinces and their inferred environments in the Indian Ocean based on distribution of Recent benthic foraminifera. Palaeogeogr Palaeoclimatol Palaeoecol 291:429–442

Diester-Haass L, Faul K (2019) Paleoproductivity reconstructions for the Paleogene Southern Ocean: a direct comparison of geochemical and micropaleontological proxies. Paleoceanogr Paleoclimatol 34:79–97. https://doi.org/10.1029/2020PA004053

EPICA community members (2004) Eight glacial cycles from an Antarctic ice core. Nature 429:623–628. https://doi.org/10.1038/nature02599

Farrell BF (1990) Equable climate dynamics. J Atmos Sci 47:2986–2995

Farrell JW, Prell WL (1989) Climatic change and CaCO₃ preservation: an 800000 year bathymetric reconstruction from the central Equatorial Pacific Ocean. Paleoceanography 4:447–446

Fedorov AV, Burls NJ, Lawrence KT, Peterson LC (2015) Tightly linked zonal and meridional sea surface temperature gradients over the past five million years. Nat Geosci 8:975–980. https://doi.org/10.1038/NGEO2577

Francois R, Honjo S, Krishfield R, Manganini S (2002) Factors controlling the flux of organic carbon to the bathypelagic zone of the ocean. Global Biogeochem Cycles 16:1087. https://doi.org/10.1029/2001GB001722

Gooday AJ (1994) The biology of deep-sea foraminifera: a review of some advances and their applications in paleoceanography. Palaios 9:14–31

Gooday AJ (2003) Benthic foraminifera (Protista) as tools in deep-water paleoceanography: a review of environmental influences on faunal characteristics. Adv Mar Biol 46:1–90

Griffith EM, Thomas E, Lewis AR, Penman DE, Westerhold T, Winguth AME (2021) Bentho-pelagic decoupling: the marine biological carbon pump during eocene hyperthermals. Paleoceanogr Paleoclimatol 36:e2020PA004053. https://doi.org/10.1029/2020PA004053

Gupta A, Sarkar S, De S, Clemens SC, Velu A (2010) Mid-Brunhes strengthening of the Indian Ocean Dipole caused increased equatorial East African and decreased Australasian rainfall. Geophys Res Lett 37:L06706. https://doi.org/10.1029/2009GL042225

Hao Q, Wang L, Oldfield F, Guo Z (2015) Extra-long interglacial in Northern Hemisphere during MISs 15–13 arising from limited extent of Arctic ice sheets in glacial MIS 14. Sci Rep 5:12103. https://doi.org/10.1038/srep12103

Henson SA, Sanders R, Madsen E (2012) Global patterns in efficiency of particulate organic carbon export and transfer to the deep ocean. Global Biogeochem Cycles 26:01028. https://doi.org/10.1029/2011GB004099

Herguera JC, Berger W (1991) Paleoproductivity from benthonic foraminifera abundance glacial to postglacial change in the west-equatorial Pacific. Geology 19:1173–1176

Howe JNW, Piotrowski AM (2003) Atlantic deep water provenance decoupled from atmospheric CO₂ concentration during the lukewarm interglacials. Nat Commun 8:1–7. https://doi.org/10.1038/s41467-017-01939-w

Jansen HHF, Kuijpers A, Troelstra SR (1986) A mid-Brunhes climatic event: long-term changes in global atmospheric and ocean circulation. Science 232:619–622

Jones RW (1994) The challenger foraminifera. Oxford University Press, Oxford

Jorissen JJ, Fontanier C, Thomas E (2007) Paleoceanographical proxies based on deep-sea benthic foraminiferal assemblage characteristics. In: Hillaire-Marcel C, de Vernal A (eds) Proxies in Late Cenozoic Paleoceanography, vol 1. Elsevier, Amsterdam, pp 263–326

Kurbjeweit F, Schmiedl G, Schiebel R, Hemleben Ch, Pfannkuche O, Wallmann K, Schäfer P (2000) Distribution biomass and diversity of benthic foraminifera in relation to sediment geochemistry in the Arabian Sea. Deep-Sea Res II 47:2913–2955

Lie Z, Herbert TD (2004) High-resolution influence on the eastern equatorial Pacific climate in the early Pleistocene epoch. Nature 427:720–723

Lin L, Khider D, Lisiecki LE, Lawrence CE (2014) Probabilistic sequence alignment of stratigraphic records. Paleoceanography 29:976–989. https://doi.org/10.1002/2014PA002713

Lisiecki LE, Raymo ME (2005) A Pliocene-Pleistocene stack of 57 globally distributed benthic δ¹⁸O records. Paleoceanography 20:PA1003. https://doi.org/10.1029/2004PA001071

Loeblich AR Jr, Tappan H (1987) Foraminiferal genera and their classification. Van Nostrand Reinhold, New York

Mackensen A, Fütterer DK, Grobe H, Schmiedl G (1993) Benthic foraminiferal assemblages from the eastern South Atlantic Polar Front region between 35º and 57º: distribution, ecology and fossilization potential. Mar Micropaleontol 22:33–39

Mackensen A, Globe H, Kuhn G, Fütterer DK (1990) Benthic foraminiferal assemblages from the eastern Weddell Sea between 69 and 73º: distribution, ecology and fossilization potential. Mar Micropaleontol 16:241–283

Mackensen A, Schmiedl G, Harloff J, Giese M (1995) Deep-sea foraminifera in the South Atlantic Ocean: ecology and assemblage generation. Micropaleontology 41:342–358

Maeda A, Kuroyanagi A, Iguchi A, Gaye B, Rixen T, Nishi H, Kawahata H (2022) Seasonal variation of fluxes of planktic foraminiferal tests collected by a time-series sediment trap in the central Bay of Bengal during three different years. Deep-Sea Res I 183:103718

Martin JH, Knauer GA, Karl DM, Broenkow WW (1987) VERTEX: carbon cycling in the northeast Pacific. Deep-Sea Res I 34:267–285

Messie M, Chavez FP (2013) Physical-biological synchrony in the global ocean associated with recent variability in the central and western equatorial Pacific. J Geophys Res Oceans 118:3782–3794

Nomura R (1995) Paleogene to Neogene deep-sea paleoceanography in the eastern Indian Ocean: benthic foraminifera from ODP Sites 747, 757 and 758. Micropaleontology 41:251–290

Oksanen J, Blanchet G, Friendly M, Kindt R, Legendre P, McGlinn D, Minchin PR, O'Hara R B, Simpson GL, Solymons P, Stevens MHH, Szoecs E, Wagner H (2019) Vegan: community ecology package. R package version v. 2. 5-6. http://cran.r-project.org/web/packages/vegan/index.html. Accessed 25 Apr 2023.

Peterson LC (1984) Recent abyssal benthic foraminiferal biofacies of the Eastern Equatorial Indian Ocean. Mar Micropaleontol 8:479–519

Peterson LC, Prell WL (1985) Carbonate preservation and rates of climate changes: an 800 kyr record from the Indian Ocean. In: Sundquist E, Broecker W (eds) The carbon cycle and atmospheric CO₂: natural variations archean to present, geophysical monograph series, vol 32. AGU, Washington DC, pp 251–269

Pisias NG, Moore TC Jr (1981) The evolution of the Pleistocene climate: a time series approach. Earth Planet Sci Lett 52:450–458

R Development Core Team (2020) R. a language and environments for statistical computing. http://www.R-project.org/ Accessed 25 Apr 2023.

Rigwell AJ (2003) An end to the "rain ratio" reign? Geochem Geophys Geosyst 4:1–5. https://doi.org/10.1029/2003GC000512

Rixen T, Gaye B, Emeis K-C, Ramaswamy V (2019) The ballast effect of lithogenic matter and its influences on the carbon fluxes in the Indian Ocean. Biogeosciences 16:485–503

Schmiedl G, Mackensen A, Müller PJ (1997) Recent benthic foraminifera from the eastern South Atlantic Ocean: dependence on food supply and water masses. Mar Micropaleontol 32:249–287

Shannon CE, Weaver W (1949) The mathematical theory of communication. The University of Illinois Press, Urbana, pp 1–117

Shipboard Scientific Party (1989) Site 758. In: Peirce J, Weissel J et al (eds) Proc ODP, Init Repts, vol 121. College Station, TX (Ocean Drilling Program), USA pp 359–453

Smart CW, King SC, Gooday AJ, Murray JW, Thomas E (1994) A benthic foraminiferal proxy of pulsed organic matter paleofluxes. Mar Micropaleontol 23:89–99

Spratt RM, Lisiecki LE (2016) A Late Pleistocene sea level stack. Clim past 12:1079–1092

Sun X, Corliss BH, Shower WJ (2006) The effect of primary productivity and seasonality on the distribution of deep-sea benthic foraminifera in the North Atlantic. Deep-Sea Res I 53:28–47

Takata H, Cho JH, Kang J, Asahi H, Lim HS, Park Y-H, Hyun S (2022) Biotic responses of deep-sea benthic foraminifera in the equatorial Indian

Ocean during the Quaternary: influence of the ballasting effect on organic matter by calcareous plankton skeletons. Palaeogeogr Palaeoclimatol Palaeoecol 538:110724. https://doi.org/10.1016/j.palaeo.2021.110724

Takata H, Khim B-K, Hyeong K, Seo I, Huh Y, Asahi H, Lee J, Seto K (2024) Ballasting of particulate organic matter at the Ninetyeast Ridge during the mid-Brunhes dissolution interval and long-term implications for zonal change in tropical Indian oceanography. Paleoceanogr Paleoclimatol 39:e2023PA004622

Takata H, Kim HJ, Asahi H, Thomas E, Yoo CM, Chi SB, Khim B-K (2019) Central Equatorial Pacific benthic foraminifera during the mid-Brunhes dissolution interval: Ballasting of particulate organic matte by biogenic silica and carbonate. Quatern Sci Rev 210:64–79

Takata H, Yoo CM, Kim HJ, Khim B-K (2016) Latitudinal difference on benthic foraminiferal fauna along ~131∘W transect in the equatorial Pacific Ocean. Ocean Sci J 51:655–663

Thiede J (1975) Distribution of foraminifera in surface waters of a coastal upwelling area. Nature 253:712–714

Thomas E (1985) Late Eocene to recent deep-sea benthic foraminifers from the central Equatorial Pacific Ocean. In: Mayer L, Theyer F, et al (eds) Initial reports of the deep sea drilling project, vol 85, pp 655–694

Thomas E (2007) Cenozoic mass extinctions in the deep sea: what perturbs the largest habitat on Earth? Geol Soc Am Spec Paper 424:1–23

Thomas E, Booth L, Maslin M, Shackleton NJ (1995) Northeastern Atlantic benthic foraminifera during the last 45,000 years: productivity changes as seen from the bottom up. Paleoceanography 10:545–562

Thomas E, Gooday AJ (1996) Cenozoic deep-sea benthic foraminifers: tracer for changes in oceanic productivity. Geology 24:355–358

Van Morkhoven FPCM, Berggren WA, Edwards AS (1986) Cenozoic cosmopolitan deep-water benthic foraminifera. Bull Cent Rech Explor Prod Elf-Aquitaine 11:1–421

Webster PJ, Magana VO, Palmer TN, Shukla J, Tomas RA, Yanai MU, Yasunari T (1998) Monsoons: processes, predictability, and the prospects for prediction. J Geophys Res Oceans 103:14451–14510

Yasuhara M, Tittensor DP, Hillebrand H, Worm B (2017) Combining marine macroecology and palaeoecology in understanding biodiversity: microfossils as a model. Biol Rev 92:199–215

Yu P-S, Kienast M, Chen M-T, Cacho I, Flores JA (2017) Surface hydrographic and water mass variability in the eastern equatorial Pacific during interglacial-like Marine Isotope Stage 14. Quatern Int 436:45–56. https://doi.org/10.1016/j.quaint.2016.12.021

Zhang H, Luo Y, Yu J, Zhang L, Xiang R, Yu Z, Huang H (2022) Indian Ocean sedimentary calcium carbonate distribution and its implications for the glacial deep ocean circulation. Quatern Sci Rev 284:107490. https://doi.org/10.1016/j.quascirev.2022.107490

Publisher's Note